nature neuroscience

Linear transformation of thalamocortical input by intracortical excitation

Ya-tang Li[1,2], Leena A Ibrahim[1,2], Bao-hua Liu[1,2], Li I Zhang[1,3] & Huizhong Whit Tao[1,4]

Neurons in thalamorecipient layers of sensory cortices integrate thalamocortical and intracortical inputs. Although we know that their functional properties can arise from the convergence of thalamic inputs, intracortical circuits could also be involved in thalamocortical transformations of sensory information. We silenced intracortical excitatory circuits with optogenetic activation of parvalbumin-positive inhibitory neurons in mouse primary visual cortex and compared visually evoked thalamocortical input with total excitation in the same layer 4 pyramidal neurons. We found that intracortical excitatory circuits preserved the orientation and direction tuning of thalamocortical excitation, with a linear amplification of thalamocortical signals of about threefold. The spatial receptive field of thalamocortical input was slightly elongated and was expanded by intracortical excitation in an approximately proportional manner. Thus, intracortical excitatory circuits faithfully reinforce the representation of thalamocortical information and may influence the size of the receptive field by recruiting additional inputs.

Neurons in layer 4 of the primary visual cortex (V1) receive excitatory inputs from two major sources: the feedforward thalamocortical input and the intracortical input from other cortical neurons[1,2]. Since the proposal that a linear spatial arrangement of thalamic neuron receptive fields results in orientation-tuned input to simple cells was first made[3–5], the respective roles of thalamocortical and intracortical inputs in generating cortical orientation selectivity have been intensively studied[6]. In one view, the feedforward input is sufficient for generating sharp orientation selectivity[7,8]. Alternatively, the feedforward input only provides a weak orientation bias, and orientation selectivity is greatly strengthened by excitation (for example, recurrent excitation) from other cortical neurons tuned to the same orientation[9–14].

Previously, several methods have been used to silence cortical spikes and isolate thalamocortical input: pharmacological silencing of the cortex by activating $GABA_A$ receptors with muscimol[15,16], cooling of the cortex[7] and electrical shocks in the cortex to produce an inhibitory widow of hundreds of milliseconds during which spikes cannot be generated[8]. Results from these studies are generally consistent with the notion that neurons in layer 4 inherit their functional properties from the relay of thalamic inputs. However, as a result of the technical limitations in previous studies (such as the nonspecific effects on synaptic transmission[17,18] or difficulties of reversible applications[15]), the precise contributions of thalamocortical and intracortical circuits to cortical orientation selectivity and other functional properties remain to be determined. Optogenetic approaches[19,20] provide an unprecedented advantage in addressing this question, as specific activation of parvalbumin (PV)-positive inhibitory neurons alone can effectively and reversibly silence spiking of cortical excitatory neurons[21]. We combined *in vivo* whole-cell voltage-clamp recordings with optical activation of PV^+ inhibitory neurons to isolate thalamocortical excitation from total excitation in the same neuron. We found that intracortical excitatory circuits preserved the orientation and direction tuning of feedforward input by linearly amplifying its signals and expanded the spatial visual receptive field by recruiting more distant inputs possibly via horizontal circuits.

RESULTS

Optogenetic silencing of visual cortical circuits

For optogenetic silencing, we used Cre-*loxP* recombination to express channelrhodopsin-2 (ChR2) in PV^+ inhibitory neurons (Online Methods). We injected an adeno-associated viral vector, AAV2/9-EF1α-DIO-ChR2-EYFP, into the V1 of *Pvalb-cre* tdTomato mice. EYFP fluorescence in cortical slices from mice 2 weeks after the injection revealed that ChR2 was expressed across cortical layers (**Fig. 1a**) and specifically in PV^+ neurons (**Fig. 1a**). We illuminated the exposed visual cortical surface with blue LED light (470 nm) via an optical fiber. In the V1 region expressing EYFP, we carried out *in vivo* cell-attached recordings from excitatory neurons to examine the effects of optical activation of PV^+ neurons. We found that LED illumination resulted in complete silencing of visually evoked spikes shortly after its onset and that the effect was sustained throughout the duration of the illumination (**Fig. 1b**). We observed such a silencing effect throughout layers 4–6 (**Fig. 1b**). To confirm that the silencing effect was a result of activating PV^+ inhibitory neurons, we carried out visually guided recordings from PV^+ neurons using two-photon imaging[22,23] (Online Methods). We found that, opposite of the effect on excitatory neurons, LED illumination markedly increased the firing rate of PV^+ neurons (**Fig. 1c**). After an initial slight reduction, the

[1]Zilkha Neurogenetic Institute, Keck School of Medicine, University of Southern California, Los Angeles, California, USA. [2]Graduate Programs, Keck School of Medicine, University of Southern California, Los Angeles, California, USA. [3]Department of Physiology and Biophysics, Keck School of Medicine, University of Southern California, Los Angeles, California, USA. [4]Department of Cell and Neurobiology, Keck School of Medicine, University of Southern California, Los Angeles, California, USA. Correspondence should be addressed to H.W.T. (htao@usc.edu).

Received 30 April; accepted 15 July; published online 11 August 2013; doi:10.1038/nn.3494

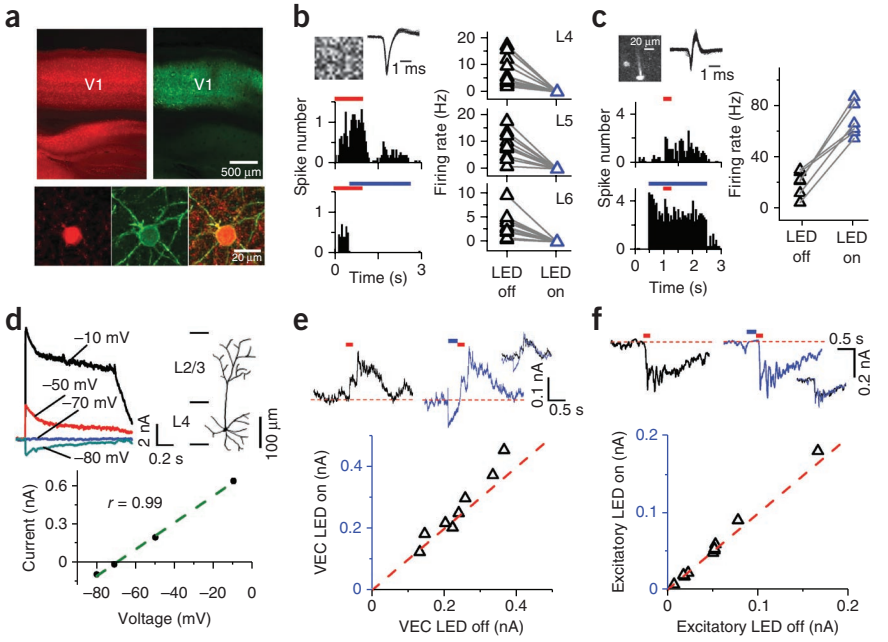

Figure 1 Optogenetic silencing of visual cortical circuits. (**a**) Top, confocal images showing tdTomato (red) and ChR2-EYFP expression (green) patterns. Bottom, enlarged images. (**b**) Left, peri-stimulus spike time histograms (PSTHs) for responses of a layer 4 excitatory neuron to a flash noise stimulus (red bar) with and without LED illumination (blue bar). Top, visual stimulus pattern and superimposed 50 individual spikes. Right, average firing rates in LED off and LED on trials for cells in different layers ($n = 14$, 10 and 11 cells from L4, L5 and L6 from 6, 5 and 5 mice, respectively). (**c**) Left, PSTHs for responses of a tdTomato-labeled PV$^+$ neuron. Top inset, two-photon image of the recorded cell and superimposed 100 individual spikes. Right, average firing rates for 6 PV$^+$ cells from 6 mice. (**d**) Top, LED illumination–induced currents in a cell and its reconstructed morphology. Bottom, current amplitude (averaged in a 40-ms window) versus holding voltage (one sided, $P = 0.005$). (**e**) Top, visually evoked ensemble currents (VECs) recorded in layer 4 without (left) and with (right) preceding LED illumination. Inset, superimposed traces. Bottom, peak amplitudes in LED on versus LED off trials (0.26 ± 0.11 versus 0.24 ± 0.08 nA, $P = 0.07$, two-tailed paired t test, $n = 8$ sites from 8 mice). (**f**) Top, visually evoked excitatory currents without and with a preceding LED illumination. Bottom, peak amplitudes in LED on versus LED off trials (median = 0.051 versus 0.051 nA, $P = 0.23$, two-sided Wilcoxon signed-rank test, $n = 10$ cells from 10 mice).

high firing rate could be maintained throughout the duration of LED illumination, which lasted for a few seconds (**Fig. 1c**). Furthermore, whole-cell voltage-clamp recordings from excitatory neurons revealed that LED illumination alone induced a large sustained current, the reversal potential of which was consistent with that of Cl^- currents (**Fig. 1d**). These results indicate that optogenetic activation of PV$^+$ inhibitory neurons effectively silences spiking of cortical excitatory neurons and therefore eliminates intracortical connections.

Previous studies in auditory and visual cortices have suggested that thalamocortical axon terminals contain $GABA_B$ receptors[17,18]. Activation of these presynaptic receptors by GABA agonists such as muscimol can reduce transmitter release[15,16]. We examined whether optogenetic activation of PV$^+$ neurons could potentially lead to a reduction of thalamocortical transmission caused by a spillover of GABA released from inhibitory synapses made by PV$^+$ cells. We recorded extracellular ensemble currents evoked by flash noise stimuli in layer 4 (Online Methods), which reflect the summed neuronal and synaptic activity in a local cortical area[24]. We then delivered LED light immediately before the visual stimulus. If there was a reduction of presynaptic release, we would expect to see a decrease in the visually evoked ensemble current. This effect was also expected to last for 1–2 s, as the decay time constant for $GABA_B$ receptors is 2.8 s (ref. 25). We found that LED illumination directly induced a negative ensemble current (**Fig. 1e**). Nevertheless, the amplitude of the following visually evoked current was not apparently reduced and its temporal profile was not altered (**Fig. 1e**). In addition, we examined visually evoked excitatory currents in layer 4 neurons, applying similar visual stimulation with and without coupling LED illumination (**Fig. 1f**). Again, we did not observe a reduction of the visually evoked excitatory currents in individual cortical cells (**Fig. 1f**). Altogether, these control experiments suggest that there is no presynaptic inhibition caused by LED-induced GABA release, possibly because GABAergic synapses made by PV$^+$ neurons are relatively distant from thalamocortical synapses. Thus, optogenetic activation of PV$^+$ neurons could be an effective method of silencing the cortex without substantially affecting thalamocortical transmission.

Scaling of orientation-tuned thalamocortical input

We next examined excitatory synaptic responses to single drifting bars at 12 different directions with and without coupling LED illumination. We carried out *in vivo* whole-cell voltage-clamp recordings with a Cs^+-based internal solution from layer 4 excitatory neurons (**Supplementary Fig. 1a**) and clamped the cells at the reversal potential for inhibitory currents, which was determined from LED-evoked currents (**Fig. 1d**). We interleaved control trials with visual stimulus only and trials in which PV$^+$ neuron were photostimulated. As shown in an example cell, LED illumination reduced the amplitude of excitatory currents to all directions of bar movement (**Fig. 2a**). In addition to the change in amplitude, we observed that the response onset latencies were prolonged (**Fig. 2a**). To quantify orientation tuning, we measured peak current amplitudes after smoothing the current traces with a 40-ms sliding window for averaging. Despite the general reduction in amplitude after cortical silencing, there was little change in orientation tuning of excitatory input, as shown by the normalized tuning curves (**Fig. 2a**). This result suggests that the excitatory responses were reduced by a similar fraction across orientations. In another word, tuning curve was scaled down. We quantified the scaling factor from the slope of linear fitting of response amplitudes in LED stimulation versus control trials (**Fig. 2a**). As shown by the example cell, the data were well fitted by a linear relationship and the scaling factor was well below 1 (**Fig. 2a**). In general, tuning shapes looked similar without and with LED illumination, with response amplitudes clearly reduced (**Fig. 2b**).

We averaged the normalized excitatory tuning curves of all of the recorded cells (19 cells from 19 mice). This population tuning curve was largely unchanged after cortical silencing (**Fig. 2c**), supporting the notion of scaling. It is worth noting that the isolated thalamocortical input (as well as the total excitatory input) was weakly tuned, with

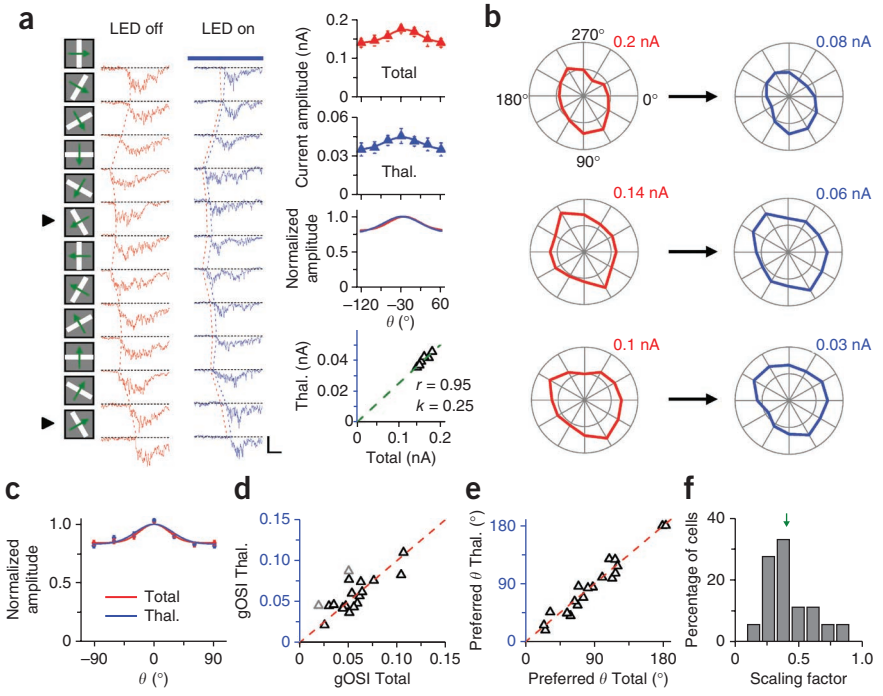

Figure 2 Linear amplification of orientation-tuned thalamocortical input. (**a**) Left, average excitatory responses (five trials) of a cell to single drifting bars at 12 different directions. Arrowheads mark the preferred orientation. Red and blue dashed curves mark the response onsets. Scale bars represent 0.1 (red) and 0.04 (blue) nA, and 0.5 s. Top right, orientation tuning curves of peak current amplitude for the total and thalamocortical (Thal.) excitation, as well as superimposed normalized tuning curves. Error bars represent s.d. Bottom right, peak current amplitudes at six orientations of LED on versus LED off trials. Dashed line indicates the linear fitting: k is the slope, r is the correlation coefficient, one-sided $P = 0.0009$. (**b**) Polar plots of excitatory current amplitude before (red) and after (blue) silencing the cortex for another three cells. The maximum axis value is labeled. (**c**) Average normalized orientation tuning curves of total excitatory input (red) and of thalamocortical input (blue). Error bars represent s.e.m. $N = 19$ cells from 19 mice. (**d**) OSI of thalamocortical input versus that of total excitation (0.059 ± 0.021 versus 0.056 ± 0.023, $P = 0.4$, two-tailed paired t test, $n = 19$ cells). Light gray triangles represent individual cells that deviated significantly from the identity line ($P < 0.05$, bootstrap analysis). (**e**) Preferred orientation of thalamocortical input versus that of total excitation ($P = 0.6$, two-tailed paired t test, $n = 19$ cells). (**f**) Distribution of scaling factors in the recorded cell population. The arrow indicates the mean value.

only a small difference between the responses to the preferred and orthogonal orientations (**Fig. 2c**). To examine the change of tuning for each individual cell, we calculated a global orientation selectivity index (gOSI, equivalent to 1 – circular variance; Online Methods). We found that orientation tuning of excitatory input was not significantly changed after cortical silencing in all but two individual cells ($P > 0.05$, bootstrap analysis; **Fig. 2d**). Neither was the preferred orientation changed in individual cells (**Fig. 2e**). The slope of linear regression (that is, scaling factor) ranged from 0.19 to 0.71, with a mean of 0.38 (**Fig. 2f**). This indicates that thalamocortical input was about one third of the total excitatory input. In other words, there was a threefold amplification of thalamocortical signals by intracortical excitatory circuits. Measurements of integrated charge of synaptic currents also supported the notion that the tuning sharpness, as well as the preferred orientation, was preserved after silencing the cortex (**Supplementary Fig. 2a,b**), although the tuning of integrated charge was weaker than that measured with peak amplitude ($P = 0.018$, one-tailed paired t test, $n = 19$ cells from 19 mice, comparison was made for responses in control trials).

Under our current recording conditions, the linear I-V relationship and the proximity of the derived reversal potential of LED-evoked currents to the expected reversal potential of inhibitory currents (**Fig. 1d**) suggest that the somatic voltage clamp was adequate. Thus, synaptic inputs relatively close to the soma might be reasonably well clamped. The thalamocortical input to layer 4 neurons, synapses of which are located proximal to the soma, is expected to be better clamped and less affected by space-clamp errors and cable attenuation compared with inputs onto distal dendrites (see Online Methods). Nevertheless,

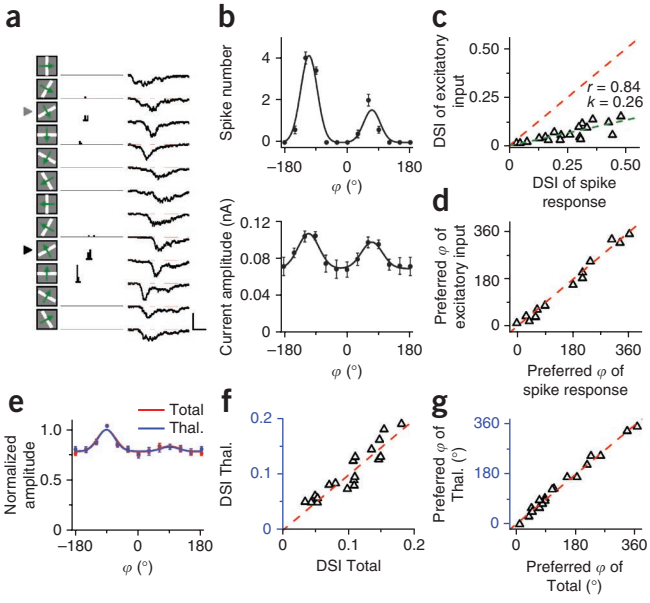

Figure 3 Intracortical excitation preserves direction tuning. (**a**) PSTH for spike responses (left, ten trials) to single drifting bars of an example layer 4 cell as well as its average excitatory responses (right, ten trials) recorded under voltage clamp. Scale bars represent 30 Hz (left) and 0.1 nA (right), 0.5 s. (**b**) Top, tuning curve of average spike count (ten trials) for the same cell. Bottom, tuning curve of average peak excitatory current. Error bars represent s.d. (**c**) DSI of excitatory input versus that of spike response ($n = 20$ cells from 20 mice). Linear fitting (olive dashed line): one-sided $P = 10^{-5}$. (**d**) Preferred direction of excitatory input versus that of spike response for cells with DSI > 0.2 ($P = 0.3$, two-tailed paired t test, $n = 13$ cells from 13 mice). (**e**) Average normalized direction tuning curves for total excitation (red) and thalamocortical excitation (blue). Error bars represent s.e.m. $N = 19$ cells from 19 mice. (**f**) DSI for thalamocortical excitation versus that for total excitation (0.104 ± 0.045 versus 0.102 ± 0.043, $P = 0.49$, two-tailed paired t test, $n = 19$ cells from 19 mice). (**g**) Preferred direction of thalamocortical excitation versus that of total excitation ($P = 0.86$, two-tailed paired t test, $n = 19$ cells).

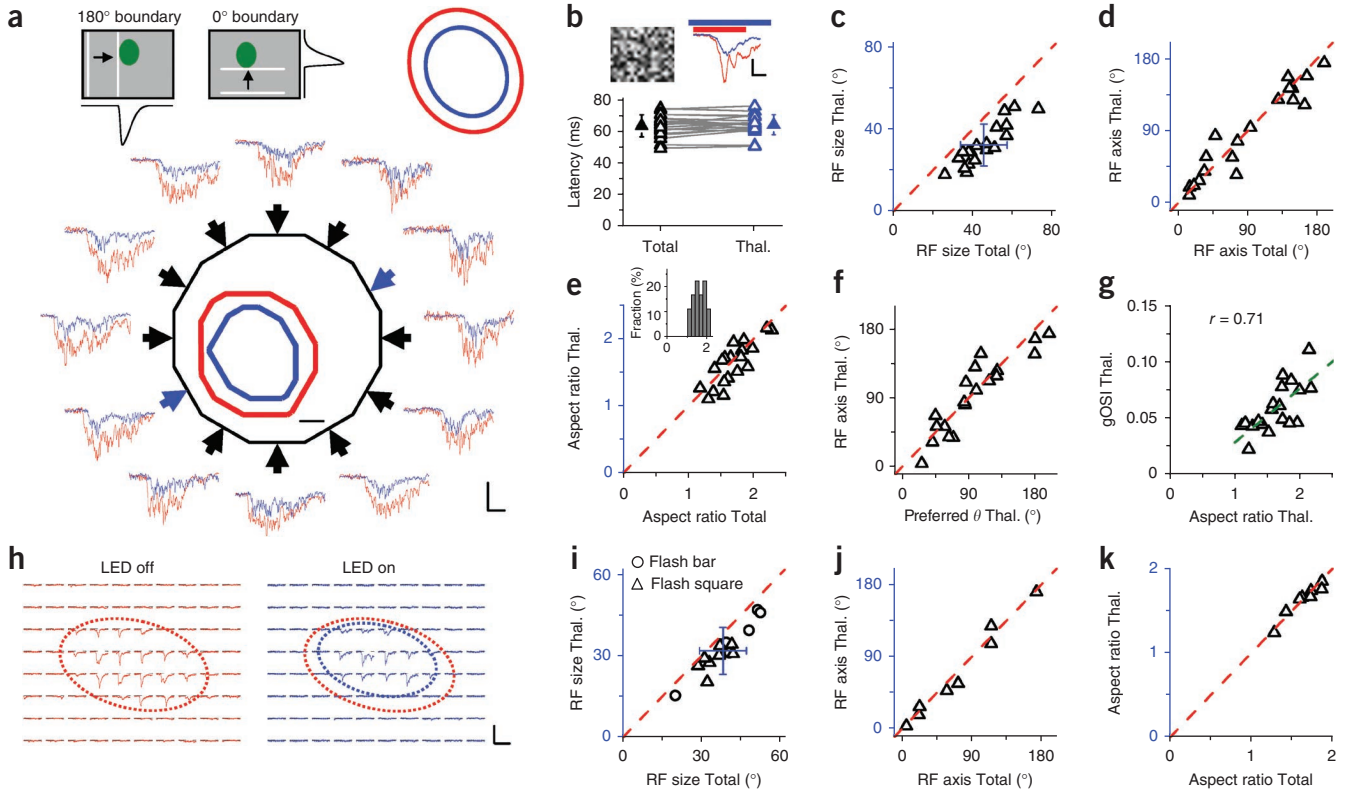

Figure 4 Intracortical excitation expands visual receptive field. (**a**) Top left, stimulation of receptive field (green) boundary correlated with the response delay. Bottom, superimposed average bar-evoked excitatory currents without (red) and with (blue) LED illumination. Scale bars represent 0.1 nA (red) and 0.05 nA (blue), and 0.5 s. Inside dodecagon, derived receptive fields before (red) and after (blue) cortical silencing. Scale bar represents 10°. Top right, elliptical fitting of the receptive fields. (**b**) Top, average excitatory currents to a flash noise stimulus. Scale bars represent 50 pA and 50 ms. Bottom, onset latencies in LED off versus LED on trials (64.1 ± 6.9 versus 64.8 ± 6.3 ms, $P = 0.32$, two-tailed paired t test, $n = 19$ cells from 19 mice; the same test applied below). Error bars represent s.d. (**c**) Receptive field (RF) size derived for thalamocortical and total excitation (mean ± s.d. marked). (**d**) Angle of receptive field major axis ($P = 0.52$). (**e**) Aspect ratio (1.63 ± 0.32 versus 1.68 ± 0.29). Inset, distribution of aspect ratios of thalamocortical receptive fields. (**f**) Derived major receptive field axis versus measured preferred orientation ($P = 0.54$). (**g**) OSI versus aspect ratio. Linear fitting: one-sided $P = 3.3 \times 10^{-4}$. (**h**) Excitatory currents of an example cell to single flash squares at different locations without and with LED stimulation. Scale bars represent 0.1 nA (left) and 0.052 nA (right), and 0.2 s. (**i**–**k**) Receptive fields measured by flash stimuli (mean ± s.d. marked; $n = 14$ cells from 14 mice). $P = 0.4$ in **j**. Aspect ratios = 1.60 ± 0.21 versus 1.58 ± 0.21, $P = 0.46$ (**k**).

we recognize that there are potential deviations of measured synaptic amplitude from the bona fide amplitude caused by space-clamp errors and cable attenuation, which need to be investigated in the future.

Intracortical excitation preserves direction tuning

Layer 4 neurons exhibit not only orientation selectivity but also direction selectivity[22,26]. To understand the relationship between direction selectivity of spike response and that of excitatory input, we carried out sequential cell-attached and whole-cell recordings (with a K^+-based internal solution) from the same neurons in wild-type mice (Online Methods). The spikes recorded in the cell-attached mode allowed us to quantify the direction selectivity of the cell's output response and the subsequent whole-cell recording allowed us to examine the underlying excitatory drive. An example cell (**Fig. 3a**,**b**) exhibited clearly direction-selective spike responses, but the amplitude of excitatory current only showed a slight difference between the preferred and null directions. Thus, consistent with what has been previously reported, the spike threshold greatly amplified the selectivity of output response[27]. The plot of direction selectivity index (DSI) of spike response versus that of excitatory current revealed a strong linear relationship (**Fig. 3c**). In addition, the preferred direction of spike response was essentially the same as that of excitatory drive (**Fig. 3d**). These results indicate that the selectivity of spike response strongly correlates with that of excitatory input, which might be employed to predict direction selectivity of the neurons.

We next examined how direction tuning of excitatory drive is determined by thalamocortical and intracortical inputs. We found that the direction tuning of excitatory drive was not changed by silencing intracortical inputs, as shown by the superimposed average direction tuning curves without and with LED illumination (**Fig. 3e**). On an individual cell basis, DSI of thalamocortical excitation was also similar to that of total excitation (**Fig. 3f**) and the preferred direction was unchanged after silencing the cortex (**Fig. 3g**). Similar conclusions could be made when the integrated charge of excitatory current was considered (**Supplementary Fig. 2c**,**d**). Together, these results suggest a linear amplification effect of intracortical excitatory circuits. The feedforward input to layer 4 neurons is already direction tuned, and the intracortical excitation increases the gain of the signal without affecting its tuning property.

Intracortical excitation expands visual receptive field

Taking advantage of drifting-bar evoked responses, we were able to estimate the shape and size of the spatial receptive field of excitatory drive. We estimated the receptive field boundary on the basis of the

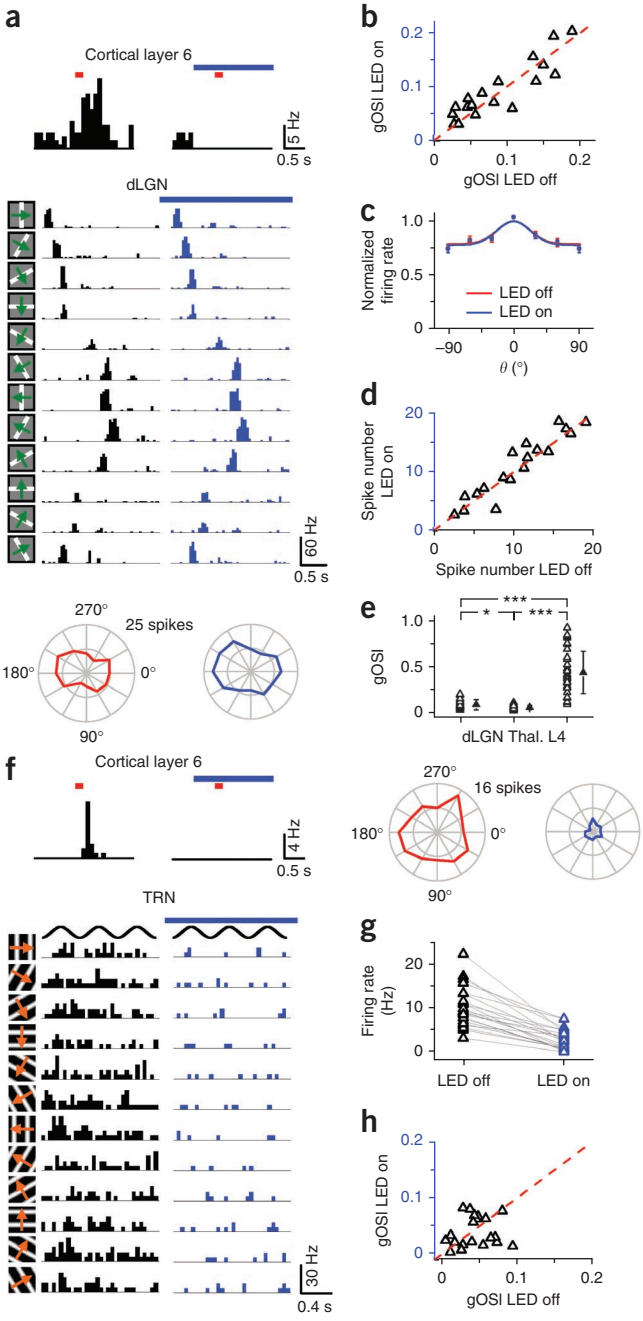

Figure 5 Orientation tuning of thalamic neurons. (**a**) Top, PSTHs for visually evoked spikes in a layer 6 neuron. Middle, PSTHs for responses to drifting bars without (black) and with (blue) LED illumination of a dLGN neuron in the same mouse. Bottom, polar plots of average spike count. (**b**) OSI of dLGN neuron responses (LED on, 0.093 ± 0.052; LED off, 0.089 ± 0.054; $P = 0.48$, two-tailed paired t test, $n = 18$ cells from 12 mice). (**c**) Average normalized tuning curves for dLGN neurons. Error bars represent s.e.m. (**d**) Evoked spike numbers for dLGN neurons (LED on, 10.4 ± 4.9; LED off, 10.9 ± 5.3; $P = 0.27$, two-tailed paired t test, $n = 18$ cells from 12 mice). (**e**) Distribution of OSIs for dLGN neuron spikes, thalamocortical excitation and layer 4 neuron spikes to drifting bars ($n = 18$, 19 and 33 cells from 12, 19 and 25 mice, respectively). $^{***}P = 5.4 \times 10^{-10}$ and 1.4×10^{-11} (top); $^{*}P = 0.022$, one-way ANOVA *post hoc* test (Tamhane's T2 test). Error bars represent s.d. (**f**) Spike responses of an example TRN neuron to drifting gratings (three cycles). Data are presented as in **a**. (**g**) Average evoked firing rates of TRN neurons (LED on, 2.8 ± 2.3; LED off, 10.2 ± 4.6 Hz; $P = 3.6 \times 10^{-9}$, one-tailed paired t test, $n = 20$ cells from 16 mice). (**h**) OSI of TRN neuron responses (LED on, 0.040 ± 0.027; LED off, 0.044 ± 0.025, $P = 0.59$, two-tailed paired t test, $n = 20$ cells from 16 mice).

moving bar speed and the response latency at each stimulus direction (**Fig. 4a**). We found that the response onset latency was prolonged in the presence of LED illumination at all stimulus directions (**Fig. 4a** and **Supplementary Fig. 3a**), suggesting that the visual receptive field had shrunk after cortical silencing. We derived receptive field outlines for the total excitation and thalamocortical excitation (Online Methods) and fitted them to an ellipse (**Fig. 4a**). We found that the derived receptive fields were both slightly elongated and the major axes of both receptive fields (that is, the axis for receptive field elongation) were similar to the preferred orientation of the cell's excitatory drive under moving stimuli (**Fig. 4a**). Our observations in this example cell suggest that the size of spatial receptive field was reduced in the presence of LED illumination, whereas its overall shape was not changed substantially.

In 19 recorded cells, we observed that the onset latency of excitatory responses to moving bars (averaged for two opposite directions) increased more for the preferred than for the orthogonal orientation (**Supplementary Fig. 3b**), suggesting that there was more receptive field shrinkage along the preferred orientation. As a control, the onset of responses to flash stimuli was not changed in the presence of LED illumination (**Fig. 4b**), indicating that the subcortical conduction of visual signals was not affected by the cortical silencing. From the response onset latencies, the estimated receptive field size (defined as the long axis of the fitted ellipse) for total excitatory input was 45.6 ± 11.7° (mean ± s.d.). The estimated receptive field was reduced to 32.4 ± 10.2° after cortical silencing ($P = 5.16 \times 10^{-10}$, two-tailed paired t test, $n = 19$ cells from 19 mice; **Fig. 4c**). Despite the reduction in size, the receptive field shape remained roughly the same, as reflected by the largely unchanged angle of the major receptive field axis ($P = 0.52$, two-tailed paired t test; **Fig. 4d**) and the unchanged aspect ratio ($P = 0.22$, two-tailed paired t test; **Fig. 4e**), which was defined as the ratio of the length of the major versus the minor receptive field axis[5,28]. In addition, the major axis of the estimated thalamocortical receptive field had an angle similar to that of the preferred orientation of the isolated thalamocortical response (**Fig. 4f**). All of the thalamocortical receptive fields were slightly elongated, as reflected by aspect ratios larger than 1, but mostly smaller than 2, with a mean of 1.63 (**Fig. 4e**). Furthermore, there was a strong linear correlation between the orientation selectivity level of thalamocortical responses and the aspect ratio of the estimated thalamocortical receptive field (**Fig. 4g**).

To further confirm the receptive field shrinkage after cortical silencing, we applied conventional flash sparse stimuli to directly map the spatial receptive field (Online Methods). We found that the receptive field indeed appeared smaller in the presence of LED illumination (**Fig. 4h**). Summary results of 14 cells recorded from 14 mice revealed that receptive field size was significantly decreased by eliminating intracortical excitatory inputs (from 38.2 ± 9.0° to 31.8 ± 8.6°, $P = 1.92 \times 10^{-6}$, one-tailed paired t test; **Fig. 4i**), whereas the angle of receptive field major axis and the aspect ratio were unaltered ($P = 0.4$ and 0.46, two-tailed paired t test; **Fig. 4j**,**k**). Notably, in normal conditions, the receptive field size measured with sparse flash stimuli was smaller than that estimated from drifting-bar responses ($P = 0.02$, one-tailed t test), whereas they were not different in cortical silencing conditions ($P = 0.87$, two-tailed t test). Thus, the receptive field size derived from drifting-bar responses was more reduced (29.4 ± 9.8%) after cortical silencing than that derived from responses to flash stimuli (16.9 ± 8.5%, $P = 2.3 \times 10^{-4}$, one-tailed t test). One possible explanation was

that some cortical neurons providing distant intracortical inputs were sensitive to moving stimuli but could not be activated by sparse flash stimuli. Altogether, these results suggest that the spatial organization of thalamic inputs (that is, the elongated arrangement) provides a basis for the orientation tuning of thalamocortical responses and that intracortical excitatory circuits expand the visual receptive field approximately proportionally in spatial extent.

Tuning of dLGN neurons is unaffected

Previous studies have suggested that layer 6 neurons in sensory cortices project back to the thalamus and may modulate thalamic neuron activity[21,29]. To investigate the effect of silencing the cortical feedback projection on thalamic activity, we carried out cell-attached recordings in the dorsal lateral geniculate nucleus (dLGN). We found that neurons in the dLGN already exhibited moderate orientation tuning as measured by either drifting bars (**Fig. 5a–c**) or drifting sinusoidal gratings (**Supplementary Fig. 4a–c**), consistent with a recent report[30]. Their tuning was not affected by cortical silencing (**Fig. 5a–c** and **Supplementary Fig. 4a–c**), the effectiveness of which was verified in each experiment by recording in layer 6. The evoked firing rates of dLGN neurons, averaged for 12 directions, were unaltered after silencing the cortex (**Fig. 5d** and **Supplementary Fig. 4d**), indicating that the reduction of excitatory drive in cortical neurons could be attributed primarily to the elimination of intracortical inputs. The tuning strength of dLGN neuron responses was slightly stronger than that of thalamocortical input but was much weaker than that of cortical neuron spikes (**Fig. 5e**).

In contrast with dLGN neurons, the evoked firing rate of thalamic reticular nucleus (TRN) neurons was markedly reduced after silencing the cortex (**Fig. 5f,g**). These neurons essentially had no orientation tuning (**Fig. 5h**). Their average OSI was 0.044 ± 0.025 (mean ± s.d., n = 20 cells from 16 mice), significantly lower than that of dLGN neurons (P = 0.0018, one tailed t test). That the firing rate of dLGN neurons was unchanged after silencing the cortex was likely a result of a concurrent decrease of excitatory drive from layer 6 and inhibitory drive from the TRN[21,29], which also receives direct excitation from layer 6 of the cortex[21,29].

DISCUSSION

As a fundamental computational property, orientation selectivity is thought to emerge in the visual cortex. Whether its generation in the thalamorecipient neurons can be solely attributed to the spatial arrangement of feedforward thalamic inputs or intracortical circuits (in particular the local recurrent network) have an indispensible role has been widely discussed[6]. We silenced intracortical excitatory connections with an optogenetic method and found that the feedforward input to mouse layer 4 excitatory neurons was weakly orientation tuned. Intracortical excitation scaled up or linearly amplified the thalamocortical signals approximately threefold without modifying the input tuning property. Similarly, the direction tuning provided by thalamocortical input was unaffected through such signal amplification. In addition, we found that intracortical excitatory circuits enlarged the visual receptive field without substantially modifying the receptive field shape.

The linear amplification of thalamocortical responses suggests that the feedforward input, although only weakly tuned, provides an orientation bias for driving orientation selectivity in the cortex. The tuning of thalamocortical input can be contributed by several mechanisms. First, the thalamocortical receptive field was slightly elongated and the axis of elongation was the same as the preferred orientation of thalamocortical responses to drifting bars. These results are consistent with the original feedforward model that the spatial organization of thalamic inputs provides a fundamental basis for orientation tuning[3]. As a result of the elongated spatial arrangement of thalamic inputs, a bar of preferred orientation can activate thalamic inputs more synchronously than a bar of orthogonal orientation. More synchronous inputs can generate a larger peak current and can be more efficient in driving spiking of layer 4 cells[31]. Second, dLGN neurons themselves were orientation tuned. The convergence of LGN inputs with similar orientation preference might be sufficient for providing orientation-tuned input to a cortical neuron. However, without understanding the relationship between orientation preferences of LGN neurons and their cortical targets, the contribution of tuning of individual LGN neurons remains unclear. Furthermore, the segregation of ON and OFF thalamic inputs[6,32], which we did not examine, may also contribute to the orientation tuning of the summed thalamocortical input.

Previous studies in cat visual cortex have focused on membrane potential responses[7,8], which reflect a result of the interaction between excitatory and inhibitory inputs. The combining of optogenetic silencing with voltage-clamp recordings allows the direct elucidation of different excitatory components and determination of their contributions to cortical functional properties. As has been seen in the cat visual cortex, we found no evidence that intracortical excitatory circuits substantially sharpen orientation tuning, which was predicted by previous theoretical models based on recurrent circuits[9–11]. Instead, excitatory responses were scaled up by a similar factor across different orientations. Such scaling or gain modulation of feedforward thalamocortical signals determined that the total excitation remained weakly tuned. The orientation selectivity of spike responses of cortical neurons was much stronger than their thalamic inputs (**Fig. 5e**). The sharp selectivity of output response may be eventually achieved through the effects of more broadly tuned inhibition[22,33–39] and spike threshold[27,35,40–42]. In addition, nonlinear mechanisms that were not revealed by the voltage-clamp recordings, for example, NMDA receptor activation[43], may also serve to sharpen the tuning of output response.

What kind of intracortical circuits might be responsible for the multiplication of thalamocortical signals? Neurons with different orientation preference in the mouse visual cortex are organized in a random 'salt-and-pepper' pattern[34,44]. However, the connection probability between excitatory neurons with a similar preferred orientation is slightly higher than that between neurons preferring different orientations[34]. Such biased connectivity between cortical excitatory neurons is likely to be sufficient for generating the weakly tuned intracortical excitation, which is also co-tuned with the feedforward excitation. The cortical gain is roughly 2, tripling the amplitude of feedforward input. The gain modulation of excitatory drive by intracortical circuits ensures that feedforward signals are reliably and faithfully represented in the cortex.

On the other hand, intracortical circuits may provide opportunities for integrating novel information by expanding the visual receptive field. It has been thought that horizontal or lateral interactions contribute to the 'silent' extra-classical receptive field, the activation of which provides contextual information that can modulate responses to stimulation of the central classical receptive field of the cell[45–47]. Our results provide direct evidence that visual receptive field peripheries might be attributed to intracortical circuits. Notably, the recruitment of more distant inputs through intracortical circuits largely preserved the elongated shape of the receptive field, suggesting that the spatial integration of intracortical inputs had a bias along the preferred orientation of the cell. That is, there might be more inputs arranged along the preferred orientation than the orthogonal, contributing to the

tuning of intracortical excitation[48]. Such connectivity pattern may arise during development under the guidance of correlation-based Hebbian plasticity rules[49,50]. The coherent organization of thalamocortical and intracortical inputs allows cortical neurons to faithfully reinforce the representation of thalamocortical information.

METHODS

Methods and any associated references are available in the online version of the paper.

Note: Any Supplementary Information and Source Data files are available in the online version of the paper.

ACKNOWLEDGMENTS

We thank M. Scanziani for the help on viral injection setup. This work was supported by grants to H.W.T. from the US National Institutes of Health (EY019049 and EY022478) and the Kirchgessner Foundation.

AUTHOR CONTRIBUTIONS

H.W.T. conceived and designed the study. Y.L. and L.A.I. performed the experiment. Y.L. and L.I.Z. performed data analysis. B.L. contributed data on direction tuning. H.W.T. wrote the paper.

COMPETING FINANCIAL INTERESTS

The authors declare no competing financial interests.

1. Douglas, R.J. & Martin, K.A. A functional microcircuit for cat visual cortex. *J. Physiol. (Lond.)* **440**, 735–769 (1991).
2. Callaway, E.M. Local circuits in primary visual cortex of the macaque monkey. *Annu. Rev. Neurosci.* **21**, 47–74 (1998).
3. Hubel, D.H. & Wiesel, T.N. Receptive fields, binocular interaction and functional architecture in the cat's visual cortex. *J. Physiol. (Lond.)* **160**, 106–154 (1962).
4. Reid, R.C. & Alonso, J.M. Specificity of monosynaptic connections from thalamus to visual cortex. *Nature* **378**, 281–284 (1995).
5. Lampl, I., Anderson, J.S., Gillespie, D.C. & Ferster, D. Prediction of orientation selectivity from receptive field architecture in simple cells of cat visual cortex. *Neuron* **30**, 263–274 (2001).
6. Ferster, D. & Miller, K.D. Neural mechanisms of orientation selectivity in the visual cortex. *Annu. Rev. Neurosci.* **23**, 441–471 (2000).
7. Ferster, D., Chung, S. & Wheat, H. Orientation selectivity of thalamic input to simple cells of cat visual cortex. *Nature* **380**, 249–252 (1996).
8. Chung, S. & Ferster, D. Strength and orientation tuning of the thalamic input to simple cells revealed by electrically evoked cortical suppression. *Neuron* **20**, 1177–1189 (1998).
9. Ben-Yishai, R., Bar-Or, R.L. & Sompolinsky, H. Theory of orientation tuning in visual cortex. *Proc. Natl. Acad. Sci. USA* **92**, 3844–3848 (1995).
10. Somers, D.C., Nelson, S.B. & Sur, M. An emergent model of orientation selectivity in cat visual cortical simple cells. *J. Neurosci.* **15**, 5448–5465 (1995).
11. Douglas, R.J., Koch, C., Mahowald, M., Martin, K.A. & Suarez, H.H. Recurrent excitation in neocortical circuits. *Science* **269**, 981–985 (1995).
12. Ben-Yishai, R., Hansel, D. & Sompolinsky, H. Traveling waves and the processing of weakly tuned inputs in a cortical network module. *J. Comput. Neurosci.* **4**, 57–77 (1997).
13. Adorján, P., Levitt, J.B., Lund, J.S. & Obermayer, K. A model for the intracortical origin of orientation preference and tuning in macaque striate cortex. *Vis. Neurosci.* **16**, 303–318 (1999).
14. McLaughlin, D., Shapley, R., Shelley, M. & Wielaard, D.J. A neuronal network model of macaque primary visual cortex (V1): orientation selectivity and dynamics in the input layer 4Calpha. *Proc. Natl. Acad. Sci. USA* **97**, 8087–8092 (2000).
15. Liu, B.H., Wu, G.K., Arbuckle, R., Tao, H.W. & Zhang, L.I. Defining cortical frequency tuning with recurrent excitatory circuitry. *Nat. Neurosci.* **10**, 1594–1600 (2007).
16. Khibnik, L.A., Cho, K.K. & Bear, M.F. Relative contribution of feedforward excitatory connections to expression of ocular dominance plasticity in layer 4 of visual cortex. *Neuron* **66**, 493–500 (2010).
17. Yamauchi, T., Hori, T. & Takahashi, T. Presynaptic inhibition by muscimol through GABAB receptors. *Eur. J. Neurosci.* **12**, 3433–3436 (2000).
18. Porter, J.T. & Nieves, D. Presynaptic GABAB receptors modulate thalamic excitation of inhibitory and excitatory neurons in the mouse barrel cortex. *J. Neurophysiol.* **92**, 2762–2770 (2004).
19. Zhang, F., Aravanis, A.M., Adamantidis, A., de Lecea, L. & Deisseroth, K. Circuit-breakers: optical technologies for probing neural signals and systems. *Nat. Rev. Neurosci.* **8**, 577–581 (2007).
20. Bernstein, J.G., Garrity, P.A. & Boyden, E.S. Optogenetics and thermogenetics: technologies for controlling the activity of targeted cells within intact neural circuits. *Curr. Opin. Neurobiol.* **22**, 61–71 (2012).
21. Olsen, S.R., Bortone, D.S., Adesnik, H. & Scanziani, M. Gain control by layer six in cortical circuits of vision. *Nature* **483**, 47–52 (2012).
22. Ma, W.P. *et al.* Visual representations by cortical somatostatin inhibitory neurons—selective, but with weak and delayed responses. *J. Neurosci.* **30**, 14371–14379 (2010).
23. Liu, B.H. *et al.* Visual receptive field structure of cortical inhibitory neurons revealed by two-photon imaging guided recording. *J. Neurosci.* **29**, 10520–10532 (2009).
24. Katzner, S. *et al.* Local origin of field potentials in visual cortex. *Neuron* **61**, 35–41 (2009).
25. Pfrieger, F.W., Gottmann, K. & Lux, H.D. Kinetics of GABAB receptor–mediated inhibition of calcium currents and excitatory synaptic transmission in hippocampal neurons in vitro. *Neuron* **12**, 97–107 (1994).
26. Niell, C.M. & Stryker, M.P. Highly selective receptive fields in mouse visual cortex. *J. Neurosci.* **28**, 7520–7536 (2008).
27. Priebe, N.J. & Ferster, D. Inhibition, spike threshold, and stimulus selectivity in primary visual cortex. *Neuron* **57**, 482–497 (2008).
28. Volgushev, M., Vidyasagar, T.R. & Pei, X. A linear model fails to predict orientation selectivity of cells in the cat visual cortex. *J. Physiol. (Lond.)* **496**, 597–606 (1996).
29. Cruikshank, S.J., Urabe, H., Nurmikko, A.V. & Connors, B.W. Pathway-specific feedforward circuits between thalamus and neocortex revealed by selective optical stimulation of axons. *Neuron* **65**, 230–245 (2010).
30. Piscopo, D.M., El-Danaf, R.N., Huberman, A.D. & Niell, C.M. Diverse visual features encoded in mouse lateral geniculate nucleus. *J. Neurosci.* **33**, 4642–4656 (2013).
31. Bruno, R.M. & Sakmann, B. Cortex is driven by weak but synchronously active thalamocortical synapses. *Science* **312**, 1622–1627 (2006).
32. Jin, J., Wang, Y., Swadlow, H.A. & Alonso, J.M. Population receptive fields of ON and OFF thalamic inputs to an orientation column in visual cortex. *Nat. Neurosci.* **14**, 232–238 (2011).
33. Kerlin, A.M., Andermann, M.L., Berezovskii, V.K. & Reid, R.C. Broadly tuned response properties of diverse inhibitory neuron subtypes in mouse visual cortex. *Neuron* **67**, 858–871 (2010).
34. Ko, H. *et al.* Functional specificity of local synaptic connections in neocortical networks. *Nature* **473**, 87–91 (2011).
35. Liu, B.H. *et al.* Broad inhibition sharpens orientation selectivity by expanding input dynamic range in mouse simple cells. *Neuron* **71**, 542–554 (2011).
36. Li, Y.T. *et al.* Broadening of inhibitory tuning underlies contrast-dependent sharpening of orientation selectivity in mouse visual cortex. *J. Neurosci.* **32**, 16466–16477 (2012).
37. Atallah, B.V., Bruns, W., Carandini, M. & Scanziani, M. Parvalbumin-expressing interneurons linearly transform cortical responses to visual stimuli. *Neuron* **73**, 159–170 (2012).
38. Wilson, N.R., Runyan, C.A., Wang, F.L. & Sur, M. Division and subtraction by distinct cortical inhibitory networks *in vivo*. *Nature* **488**, 343–348 (2012).
39. Lee, S.H. *et al.* Activation of specific interneurons improves V1 feature selectivity and visual perception. *Nature* **488**, 379–383 (2012).
40. Liu, B.H. *et al.* Intervening inhibition underlies simple-cell receptive field structure in visual cortex. *Nat. Neurosci.* **13**, 89–96 (2010).
41. Tan, A.Y., Brown, B.D., Scholl, B., Mohanty, D. & Priebe, N.J. Orientation selectivity of synaptic input to neurons in mouse and cat primary visual cortex. *J. Neurosci.* **31**, 12339–12350 (2011).
42. Katzner, S., Busse, L. & Carandini, M. GABAA inhibition controls response gain in visual cortex. *J. Neurosci.* **31**, 5931–5941 (2011).
43. Branco, T., Clark, B.A. & Hausser, M. Dendritic discrimination of temporal input sequences in cortical neurons. *Science* **329**, 1671–1675 (2010).
44. Ohki, K., Chung, S., Ch'ng, Y.H., Kara, P. & Reid, R.C. Functional imaging with cellular resolution reveals precise micro-architecture in visual cortex. *Nature* **433**, 597–603 (2005).
45. Allman, J., Miezin, F. & McGuinness, E. Stimulus specific responses from beyond the classical receptive field: neurophysiological mechanisms for local-global comparisons in visual neurons. *Annu. Rev. Neurosci.* **8**, 407–430 (1985).
46. Gilbert, C.D. & Wiesel, T.N. The influence of contextual stimuli on the orientation selectivity of cells in primary visual cortex of the cat. *Vision Res.* **30**, 1689–1701 (1990).
47. Levitt, J.B. & Lund, J.S. Contrast dependence of contextual effects in primate visual cortex. *Nature* **387**, 73–76 (1997).
48. Chisum, H.J., Mooser, F. & Fitzpatrick, D. Emergent properties of layer 2/3 neurons reflect the collinear arrangement of horizontal connections in tree shrew visual cortex. *J. Neurosci.* **23**, 2947–2960 (2003).
49. Clopath, C., Busing, L., Vasilaki, E. & Gerstner, W. Connectivity reflects coding: a model of voltage-based STDP with homeostasis. *Nat. Neurosci.* **13**, 344–352 (2010).
50. Ko, H. *et al.* The emergence of functional microcircuits in visual cortex. *Nature* **496**, 96–100 (2013).

ONLINE METHODS

All experimental procedures used in this study were approved by the Animal Care and Use Committee of the University of Southern California.

Viral injection. Female mice (45–60 d old) used in experiments were generated by crossing *Pvalb-cre* mice with tdTomato reporter mice (Jackson Laboratory, C57BL/6J background). We anesthetized mice with 2% isoflurane (vol/vol), thinned the skull over V1 and performed ~0.2-mm^2 craniotomy. We delivered the virus using a beveled glass micropipette (tip diameter = 40–50 μm) attached to a microsyringe pump (World Precision Instruments). Adeno-associated viruses (AAVs) to deliver ChR2 were acquired from the University of Pennsylvania Viral Vector Core (AAV2/9.EF1α.DIO.hChR2(H134R)-EYFP.WPRE.hGH, Addgene 20298). We injected virus at a volume of 50 nl per injection and at a rate of 20 nl min^{-1}. We performed the injection at two locations ([0.8, 2.3], [0.8, 3] mm anterior and lateral to lambda) and two depths (300 and 600 μm). We then sutured the scalp and administered an analgesic (0.1 mg per kg of weight Buprenex) to help the recovery from anesthesia. We made *in vivo* recordings 2–3 weeks after viral injections. We examined the expression pattern of hChR2(H134R)-EYFP in each injected mouse before the experiment, and carried out recordings only in mice with a correct location of EYFP expression (1 of 20 mice was excluded). That is, for the major experiments, there was only one mouse group. In more than 300 EYFP-expressing neurons examined in four mice, all of them expressed tdTomato, indicating that they were all PV$^+$ inhibitory neurons.

Animal surgery. We sedated the mouse with EYFP expression with an intramuscular injection of chlorprothixene hydrochloride (10 mg per kg in 4 mg ml^{-1} water solution) and then anesthetized it with urethane (1.2 g per kg, intraperitoneal, 20% (wt/vol) in saline), as previously described[23,26]. We maintained the mouse's body temperature at ~37.5° by a heating pad (Havard Apparatus). We performed tracheotomy and inserted a small glass capillary tube to maintain a free airway. We performed cerebrospinal fluid draining, removed the skull and dura mater (~1 × 1 mm) over the V1, and applied artificial cerebrospinal fluid solution (ACSF, containing 140 mM NaCl, 2.5 mM KCl, 2.5 mM $CaCl_2$, 1.3 mM $MgSO_4$, 1.0 mM NaH_2PO_4, 20 mM HEPES, 11 mM glucose, pH 7.4) to the exposed cortical surface when necessary. We trimmed eyelashes contralateral to the recording side, and covered the eyes with ophthalmic lubricant ointment until recording, at which point we rinsed the eyes with saline and applied a thin layer of silicone oil (30,000 centistokes) to prevent drying while allowing clear optical transmission. Eye movements and the receptive field drift were negligible in the time window of our recordings[40].

***In vivo* electrophysiology.** We pre-penetrated the pia with a broken pipette under visual guidance before *in vivo* recordings, and then performed whole-cell voltage-clamp recordings with an Axopatch 200B (Molecular Devices). The patch pipette had a tip opening of ~2 μm (4–5-MΩ impedance). The Cs$^+$-based intrapipette solution used for voltage-clamp recordings contained 125 mM cesium gluconate, 5 mM TEA-Cl, 4 mM MgATP, 0.3 mM GTP, 8 mM disodium phosphocreatine, 10 mM HEPES, 10 mM EGTA, 2 mM CsCl, 1 mM QX-314, 0.75 mM MK-801 and 1% biocytin (wt/vol) (pH 7.25).

The K$^+$-based intrapipette solution used for sequential cell-attached and whole-cell recordings contained 130 mM potassium gluconate, 4 mM MgATP, 0.3 mM GTP, 8 mM disodium phosphocreatine, 10 mM HEPES, 10 mM EGTA, 2 mM KCl and 1% biocytin (pH 7.25). The pipette capacitance and whole-cell capacitance were compensated completely and series resistance was compensated by 50–60% (at 100-μs lag). A –11-mV junction potential was corrected. Signals were filtered at 2 kHz and sampled at 10 kHz. We isolated excitatory currents by clamping the cell at the reversal potential for LED-evoked Cl$^-$ currents (−64 ± 6 mV), which was determined for each individual experiment. As discussed previously[36,40], our whole-cell recording method with relatively large pipettes highly biases sampling toward pyramidal neurons. For cell-attached recordings only, the pipette contained ACSF and we recorded spikes in the voltage-clamp mode, applying a small command potential to achieve a zero baseline current. The spike signal was filtered at 10 kHz and sampled at 20 kHz. The spike waveform of recorded excitatory neurons had a trough-to-peak interval of 0.85 ± 0.10 ms (n = 35 cells). We recorded the extracellular ensemble currents with a patch pipette filled with 1 M NaCl, under voltage clamp with a holding voltage of 0 mV. Signals were filtered at 10 kHz and sampled at 20 kHz.

We determined the depth location of layer 4 (370–510 μm from the pia) based on the expression pattern in a layer-4–specific Cre line (Scnn1a-Tg3-Cre, Jackson Laboratory) crossed with the tdTomato reporter line (**Supplementary Fig. 1a**). The layer assignment of the blindly recorded neurons was made mostly according to the vertical travel distance of the electrode. The assignment was reasonably precise, as our use of a high-magnification objective (40×) on the microscope allowed a precise identification of the cortical surface and our application of pre-penetration minimized the dimpling of the cortical surface. Morphologies of 15 recorded layer 4 cells were successfully reconstructed (**Fig. 1d** and **Supplementary Fig. 1**), which confirmed that they were located in layer 4.

For recording in the dLGN, we made a square craniotomy of 1.5 × 1.5 mm approximately 2.5 mm posterior and 2 mm lateral to the bregma structure. We applied cell-attached recordings to collect spikes from single neurons. The spike signal was filtered at 10 kHz and sampled at 20 kHz. We recorded from dLGN relay neurons, characterized by robust visually evoked responses with low spontaneous activity, at a depth of 2,500–3,100 μm (ref. 51). For recording in the TRN, we made a square craniotomy of 1.5 × 1.5 mm around 1.1 mm posterior and 1.6 mm lateral to the bregma structure, and carried out cell-attached recordings at a depth of 2,400–3,000 μm.

***In vivo* two-photon imaging guided recording.** We tuned a mode-locked Ti:sapphire laser (MaiTai Broadband, Spectra-Physics) at 890 nm with the output power at 60–300 mW for imaging fluorescently labeled neurons in layer 4, and adjusted the power according to the cell's fluorescence level. We filled the glass electrode, with ~1-μm tip opening and 8–10-MΩ impedance, with ACSF containing 0.15 mM calcein (Invitrogen). We completely compensated for the pipette capacitance. We navigated the pipette tip in the cortex and patched it onto a fluorescent soma as previously described[23]. After confirming a successful targeting, we released the positive pressure in the pipette (~10 mbar) and applied a negative pressure (20–150 mbar) to form a loose seal (with 80–200-MΩ resistance). We directly determined the depth of the patched cell under the two-photon microscope. The depth of the recorded PV$^+$ neurons ranged from 365–455 μm below the pia. The recorded PV$^+$ neurons all exhibited narrow spike waveforms, with an average through-to-peak interval of 0.32 ± 0.05 ms (n = 6).

Visual stimulation. We implemented the visual stimuli using MATLAB with Psychophysics Toolbox and displayed them with a gamma-corrected LCD monitor (refresh rate = 75 Hz, maximum luminance = 280 cd m^{-2}) placed 0.25 m away from the right eye. We placed the center of the monitor at 45° azimuth, 25° elevation, and it covered ±35° horizontally and ±27° vertically of the mouse visual field. We made recordings in the monocular zone of the V1. We recorded spontaneous activity by applying a uniform gray background. To measure orientation tuning, we applied drifting single bars (4° × 60°, at a speed of 50° s^{-1}) of 12 directions (30° per step) in a pseudorandom sequence. The visual stimulation with and without LED illumination were alternated, but the stimulus sequence was randomized independently for LED off and LED on trials. Thus, data collection was randomized. We set the inter-stimulus interval at 10 s to allow a full recovery of ChR2 function from desensitization[52]. We applied 5–10 sets of stimuli to each cell, with the sequence different between sets. For recordings in the dLGN and TRN, we applied both drifting bars and full-field drifting sinusoidal gratings (temporal frequency = 2 Hz, spatial frequency = 0.04 cycles per degree, 95% contrast) at 12 directions. We also mapped the receptive field with flash stimuli, either flash light squares (5° × 5°) or flash light bars (4° × 60°) of vertical orientation for 5–10 repetitions in a pseudorandom sequence.

Photostimulation. To photoactivate ChR2, we used a blue (470 nm) fiber-coupled LED (0.2-mm diameter, Doric Lenses) placed on top of the exposed cortical surface. LED light spanned the entire area of V1. We applied black pigment–stained agar to prevent LED light from scattering and reaching the contralateral eye, and had verified that LED light did not directly stimulate the eye in wild-type mice. The LED was driven by the analog output from a NIDAQ board (National Instruments). The intensity of LED was around 5 mW (measured at the tip of the fiber).

Data analysis. We performed data analysis with custom-developed software (LabVIEW, National Instrument; MATLAB, MathWorks), not blind to the conditions of the experiments. We counted the spikes evoked by drifting bars or

drifting sinusoidal gratings in a time window covering the visual stimulation duration with a 70-ms delay, and subtracted the spontaneous firing rate from the stimulus-evoked spike rate. We averaged the recorded synaptic responses, smoothing by averaging within a sliding 40-ms window[53].

We quantified the strength of orientation selectivity with a gOSI

$$\mathrm{gOSI} = \frac{\left\| \sum R(\theta) \times e^{2i\theta} \right\|}{\sum R(\theta)}$$

i is $\sqrt{-1}$. θ is the angle of the moving direction. $R(\theta)$ is the response level at angle θ. We averaged the response levels of two directions at the same orientation to obtain the orientation tuning curve between 0–180 degrees, and fitted it with a Gaussian function $R(\theta) = A \times \exp(-0.5 \times (\theta - \varphi)^2 / \sigma^2) + B$. φ is the preferred orientation. σ is the tuning width. To measure the DSI, we fitted the response levels at 12 stimulus directions to a wrapped Gaussian function $R(\theta) = A_1 \times \exp(-0.5 \times (\theta - \varphi)^2 / \sigma^2) + A_2 \times \exp(-0.5 \times (\theta - \varphi - 180°)^2 / \sigma^2) + B$. φ is the preferred direction. σ is the tuning width. DSI was defined as $(A_1 - A_2) / (A_1 + A_2 + 2B)$.

LED illumination alone led to a decrease in input resistance (from 181 ± 22 to 118 ± 24 MΩ, $P = 0.002$, one-tailed paired t test, $n = 5$ cells from 5 mice), which was measured by examining the voltage change to a 100-pA step current. We estimated how much the decrease of input resistance would affect the recorded current amplitude based on[15]

$$I_{\mathrm{rec}} = \frac{R_{\mathrm{in}}}{R_{\mathrm{in}} + R_{\mathrm{s}}} \times I_{\mathrm{syn}}$$

I_{syn} is the actual amplitude of synaptic current. I_{rec} is the recorded amplitude. R_{in} is the input resistance. R_{s} is the effective series resistance (15~30 MΩ) in our recordings, which was unchanged after cortical silencing. The decrease of R_{in} from 181 to 118 MΩ would lead to a 4~7% reduction of the recorded synaptic amplitude, which is negligible compared with the measured amplitude reduction after cortical silencing (**Fig. 2f**). It should be noted that the putative change in recorded current amplitudes resulting from the change in input resistance would not substantially affect the tuning of synaptic responses. Similarly, as we have previously discussed[15,40,54], under our recording condition, the observed synaptic responses can be reasonably controlled by the somatic voltage clamp. This was suggested by the linear *I-V* relationship and the proximity of LED-evoked currents to the expected reversal potential of inhibitory currents (**Fig. 1d**). The thalamocortical synapses on layer 4 neurons have been shown to be proximal to the soma[55]. These synaptic inputs would be less affected by changes in input resistance compared to inputs onto distal dendrites[56]. Nevertheless, potential deviations of measured synaptic amplitudes from bona fide amplitudes caused by space-clamp errors and cable attenuation should be recognized[57–59].

To derive receptive field boundaries, we translated the onset delay of each drifting-bar response (after compensation for the subcortical conduction delay as determined from the cell's response to flash noise stimuli; **Fig. 4b**) into the distance the bar had moved. To determine the response onset, we first identified the time point where the peak current occurred and then traced current backward from the peak time to the time point where the amplitude was reduced to 5% of the peak value. We also visually examined response traces to confirm the determined onsets. The lines marking the bar positions at the compensated response onsets intercepted to form a dodecagon that outlined the spatial receptive field. We determined the midpoint of each side of the dodecagon and performed the least-squares fitting to an ellipse for the 12 midpoints. We defined the receptive field size as the length of the major axis of the ellipse, and the aspect ratio as the ratio of the major versus minor axis of the ellipse.

For flash stimuli, we identified the visually evoked responses if the average peak current was 3 s.d. greater than the baseline current in the absence of visual stimuli. For synaptic responses to flash squares, we fitted the receptive field to an elliptic function and determined the receptive field boundary as previously described[29].

Statistical analysis. We first performed Shapiro-Wilk test to test whether data were normally distributed. In the case of a normal distribution, we performed a paired t test. Otherwise, we performed nonparametric tests (Wilcoxon signed-rank test in this study). In fact, nonparametric and parametric methods led to the same conclusions. For multiple comparisons of normally distributed data, we applied one-way ANOVA followed by appropriate *post hoc* tests, which was selected on the basis of the test of homogeneity of variances. Data were presented as mean ± s.d. if not otherwise specified. No statistical method was used to predetermine sample sizes, but our sample sizes were similar to those reported in previous publications in the field[8,16,37,41].

51. Grubb, M.S. & Thompson, I.D. Quantitative characterization of visual response properties in the mouse dorsal lateral geniculate nucleus. *J. Neurophysiol.* **90**, 3594–3607 (2003).
52. Lin, J.Y., Lin, M.Z., Steinbach, P. & Tsien, R.Y. Characterization of engineered channelrhodopsin variants with improved properties and kinetics. *Biophys. J.* **96**, 1803–1814 (2009).
53. Li, Y.T., Ma, W.P., Pan, C.J., Zhang, L.I. & Tao, H.W. Broadening of cortical inhibition mediates developmental sharpening of orientation selectivity. *J. Neurosci.* **32**, 3981–3991 (2012).
54. Wu, G.K., Li, P., Tao, H.W. & Zhang, L.I. Nonmonotonic synaptic excitation and imbalanced inhibition underlying cortical intensity tuning. *Neuron* **52**, 705–715 (2006).
55. Petreanu, L., Mao, T., Sternson, S.M. & Svoboda, K. The subcellular organization of neocortical excitatory connections. *Nature* **457**, 1142–1145 (2009).
56. Zhang, M. *et al.* Functional elimination of excitatory feedforward inputs underlies developmental refinement of visual receptive fields in zebrafish. *J. Neurosci.* **31**, 5460–5469 (2011).
57. Wehr, M. & Zador, A.M. Balanced inhibition underlies tuning and sharpens spike timing in auditory cortex. *Nature* **426**, 442–446 (2003).
58. Wu, G.K., Tao, H.W. & Zhang, L.I. From elementary synaptic circuits to information processing in primary auditory cortex. *Neurosci. Biobehav. Rev.* **35**, 2094–2104 (2011).
59. Tan, A.Y., Zhang, L.I., Merzenich, M.M. & Schreiner, C.E. Tone-evoked excitatory and inhibitory synaptic conductances of primary auditory cortex neurons. *J. Neurophysiol.* **92**, 630–643 (2004).